Journal of Materials Chemistry C

Accepted Manuscript

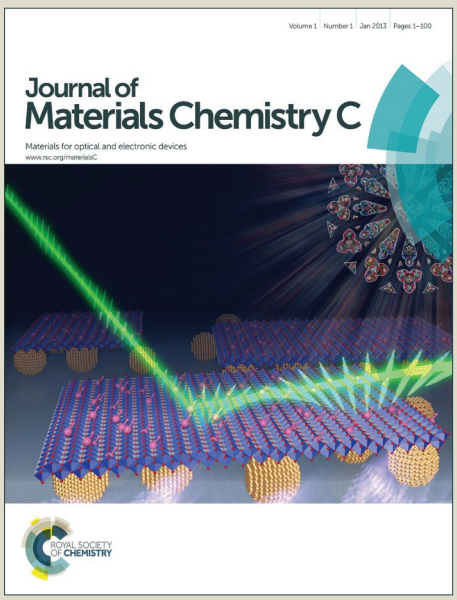

This is an *Accepted Manuscript*, which has been through the Royal Society of Chemistry peer review process and has been accepted for publication.

Accepted Manuscripts are published online shortly after acceptance, before technical editing, formatting and proof reading. Using this free service, authors can make their results available to the community, in citable form, before we publish the edited article. We will replace this *Accepted Manuscript* with the edited and formatted *Advance Article* as soon as it is available.

You can find more information about *Accepted Manuscripts* in the Information for Authors.

Please note that technical editing may introduce minor changes to the text and/or graphics, which may alter content. The journal's standard Terms & Conditions and the Ethical guidelines still apply. In no event shall the Royal Society of Chemistry be held responsible for any errors or omissions in this *Accepted Manuscript* or any consequences arising from the use of any information it contains.

ROYAL SOCIETY OF CHEMISTRY

www.rsc.org/materialsC

Hydrophobic graphene nanosheets decorated by monodispersed superparamagentic Fe_3O_4 nanocrystals as synergistic electromagnetic wave absorbers

Xinliang Zheng[a], Juan Feng[a], Yan Zong[a], Hui Miao[a], Xiaoyun Hu[a], Jintao Bai[a, b], Xinghua Li*[a]

[a] School of Physics, Northwest University, Xi'an 710069, China

[b] Institute of Photonics and Photo-Technology, Provinical Key Laboratory of Photoelectronic Technology, Northwest University, Xi'an 710069, China

* Corresponding authors: Xinghua Li (lixinghua04@gmail.com, lixinghua04@163.com)

Abstract

The comprehension of the interactions between the building blocks in the hybrids can give us an insight into the design and application of high efficient electromagnetic wave absorption materials. Herein, we report a facile in situ thermal decomposition route for the fabrication of superparamagnetic Fe_3O_4 nanocrystals anchored on the hydrophobic graphene nanosheets as synergistic electromagnetic wave absorbers. The microstructures and interactions of the Fe_3O_4/graphene hybrids are systematically investigated, which suggests that the Fe_3O_4 nanocrystals are uniformly decorated and chemically bonded on the surface of graphene nanosheets without obviously

Journal of Materials Chemistry C Accepted Manuscript

conglomeration or large vacancies. The Fe_3O_4/graphene hybrids show hydrophobic and superparamagnetic characteristics. Combing both the benefits of superparamagnetic Fe_3O_4 nanocrystals and electric graphene, the Fe_3O_4/graphene hybrids show a maximum reflection loss (RL) of -40 dB at 6.8 GHz with a matching thickness of 4.5 mm, and the effective absorption bandwidth (RL<-10 dB) is 4.6-18 GHz with the absorber thickness of only 2-5 mm. However, due to the lack of dielectric loss, only a weak RL of -5 dB is obtained in the bare Fe_3O_4 nanocrystals. The remarkably enhanced electromagnetic wave absorption properties of the Fe_3O_4/graphene hybrids are owing to the effective impedance matching and synergistic interaction. Moreover, compared with other reported graphene-based electromagnetic wave absorption materials, the hydrophobic Fe_3O_4/graphene hybrids prepared in this work are considered to be more stable and suitable to be applied in some particular environmental conditions such as raining.

Introduction

With the increasing demand for solving the growing electromagnetic interference (EMI) problems derived from the rapid development of wireless communication devices, considerable theoretical and experimental researches have been focused on the design and exploration of effective electromagnetic wave absorption materials which could effectively attenuate the electromagnetic waves by converting them into thermal energy or dissipating them through interference.[1-4] Traditionally, the high-efficiency electromagnetic wave absorption materials are requested to possess

Journal of Materials Chemistry C Accepted Manuscript

four characteristics, including strong adsorption, broad band adsorption, light weight and thin matching thickness. The complex permeability ($\mu_r = \mu' - j\mu''$) and permittivity ($\varepsilon_r = \varepsilon' - j\varepsilon''$) play a leading role on the performance of the electromagnetic wave absorption materials. Much effort have been made on the magnetic loss materials such as Fe,[5] Co,[6] Ni[7] and ferrite,[8] as well as the dielectric loss materials including ZnO,[9] TiO_2,[10] MnO_2,[11] CuS,[12] $BaTiO_3$,[13] graphene/polyaniline,[14] SiC/NiO[15] and MWCNTs/SiO_2.[16] However, the impedance match condition is usually out of balance for the unilateral magnetic or dielectric loss materials, resulting in a weak electromagnetic wave absorption performance or narrow frequency bandwidth. Therefore, the exploration of magnetic/dielectric hybrids has attracted much attention, for example, Fe_3O_4/ZnO,[17] Ni/TiO_2,[18] Ni/$BaTiO_3$,[19] Fe_xO_y/SiO_2[20] and so on, which have been proved to possess high electromagnetic wave absorption characteristics. But the large density greatly limits their potential industrial applications. To solve the above problems, decorating or coating the magnetic nanocrystals with carbon materials is believed to be a good candidate as lightweight electromagnetic wave absorbers.[21-24] Graphene is promised to be superior building blocks for constructing electromagnetic wave absorbers, owing to its remarkable physical properties including large surface area, high electrical conductivity, good thermal conductivity, flexibility and strong mechanical stiffness.[25] Therefore, decorating graphene with inorganic nanocrystals has been one of the most effective approaches to construct innovative hybrids with special properties.[26-29] Specially, taking advantage of the combined benefits of magnetic nanocrystals and conductive graphene, the magnetic

Journal of Materials Chemistry C Accepted Manuscript

nanocrystals/graphene hybrids show great potential as novel light-weight electromagnetic absorption materials.[30-50] The synergistic interaction effect between the magnetic nanocrystals and graphene may result in better absorption characteristic. The thermal energy converted by the absorbed electromagnetic wave can spread rapidly due to the remarkable thermal conductivity of graphene nanosheets. Among the magnetic component, Fe_3O_4 nanostructures have attracted extensive interest as electromagnetic wave absorbers because of their unique properties, such as moderate saturation magnetization value (M_s), high Curie temperature, good thermal stability and high chemical stability.[51] Therefore, graphene nanosheets decorated by Fe_3O_4 nanomaterials have been widely utilized as electromagnetic wave absorbers.[38-50] However, the magnetic nanocrystals supported on the graphene are generally aggregated with uneven distribution, leading to possible "dead area" with null magnetic components. Besides, for practical applications, the electromagnetic absorption materials should also possess antioxidation capability and corrosion resistant ability. However, to our best knowledge, the magnetic nanocrystals/graphene hybrids employed in above studies are usually hydrophilic or easily oxidized, which restrict their potential applications in some specific environment like humid climate. Moreover, for the magnetic nanocrystals-based absorber, a small coercivity is beneficial, which can improve the permeability and enhance the magnetic loss.[52] Therefore, superparamagnetic magnetic nanocrystals are favorable. Based on the foregoing, the development of hydrophobic Fe_3O_4/graphene hybrids in which monodispersed superparamagnetic Fe_3O_4 nanocrystals are decorated on the whole

Journal of Materials Chemistry C Accepted Manuscript

graphene nanosheets without aggregation is urgently needed for future practical applications. However, up to now, investigations on the preparation and electromagnetic wave absorption properties of such hydrophobic graphene-based hybrids have yet to report to date.

In this work, we have successfully prepared hydrophobic superparamagnetic Fe_3O_4/graphene hybrids by a facile in situ thermal decomposition route. Although the obtained hybrids show relative moderate electromagnetic wave absorption properties, several advantages make them attractive. First, the synergistic interaction between Fe_3O_4 and graphene plays a key role in the enhanced electromagnetic wave absorption. Second, the Fe_3O_4 nanocrystals are superparamagnetic which is favorable for improving absorption. Third, the monodispersed Fe_3O_4 nanocrystals are uniformly decorated on the whole graphene nanosheets without aggregation, suggesting no "dead area" of null magnetic components for absorption. Fourth, in comparison with the magnetic metal/graphene hybrids, the Fe_3O_4/graphene hybrids are antioxidized. Finally, the hybrids are hydrophobic which is beneficial for practical application. These results suggest that the novel hydrophobic magnetic graphene-based hybrids are promised to be innovative electromagnetic wave absorption materials for practical applications. In addition, the synthesis route is a promising strategy for the preparation of other hydrophobic graphene-based hybrids.

2. Experimental section

2.1 Materials

All the chemical reagents used in this work were of analytical grade without further

Journal of Materials Chemistry C Accepted Manuscript

purification. Natural graphite flake powders were purchased from Beijing Creative Biological Engineering Materials Co. Ltd. Iron acetylacetonate ($Fe(acac)_3$, 99%), oleylamine ($C_{18}H_{37}N$, 70%), benzyl ether ($C_{14}H_{14}O$, 90%) and 1-octadecene (ODE, $C_{18}H_{36}$, 90%) were bought from Aldrich.

2.2 Synthesis of hydrophobic Fe_3O_4/graphene hybrids

Graphene oxide (GO) was prepared from natural flake graphite through a modified Hummers method.[53] Fe_3O_4@graphene hybrids were fabricated by in-situ thermal decomposition route. In a typical process, 20 mg of GO was dissolved in the solvent composed of 10 ml of oleylamine and 10 ml of 1-octadecene and ultrasounded for 4 h to produce few-layer oleyamine-modified GO. Then 200 mg of $Fe(acac)_3$ was added into the above GO-contained solution and ultrasounded for another 0.5 h to make sure the precursor dissolve in the solution completely. The mixture solution was deoxidized and dehydrated at 120 ^oC for 1 h under a flow of argon, and then heated to 200 ^oC and maintained for 1 h. Finally the solution was quickly heated to 315 ^oC, and refluxed at this temperature for 2 h. When the reaction was finished, the black solution was cooled down to room temperature naturally. The Fe_3O_4/graphene hybrids were precipitated by adding ethanol, followed by centrifuging (10000 rpm, 3 min). The precipitates were washed and purified by ethanol/hexane (1:1) for several times. The Fe_3O_4/graphene hybrids were dispersed in hexane for further characterization.

2.3 Synthesis of Fe_3O_4 nanocrystals

For comparison purposes, bare Fe_3O_4 nanocrystals were fabricated by the similar thermal decomposition strategy. Typically, $Fe(acac)_3$ (2 mmol) was dissolved in 20

Journal of Materials Chemistry C Accepted Manuscript

ml of benzyl ether with 1, 2-duodecanediol (10 mmol), oleylamine (6 mmol) and oleic acid (6 mmol). The solution was then deoxidized and dehydrated at 120 ^{o}C for 1 h under Ar atmosphere. The solution was then heated to 200 ^{o}C and maintained for 2 h. Finally, the reaction mixture was heated to 290 ^{o}C and refluxed for another 2 h. The precipitation process of the bare Fe_3O_4 nanocrystals is similar with that of Fe_3O_4/graphene hybrids. The XRD pattern and TEM images of the bare Fe_3O_4 nanocrystals are shown in Fig. S1 and Fig. S2 (supporting information). The bare Fe_3O_4 nanocrystals show spherical shape with diameter of about 8 nm, which is the same with that of the Fe_3O_4 nanocrystals decorated on the graphene nanosheets.

2.4 Characterization

The morphology of the products were characterized using field-emission scanning electron microscopy (SEM, Hitachi S-4800, Japan) and high-resolution transmission electron microscope (HRTEM, FEI Tecnal G^2 F20) embedded with energy-dispersive X-Ray spectroscopy (EDX, Oxford Instrument), high angle annular dark field (HAADF) and scanning transmission electron microscopy (STEM). The crystal struccture were carried out by X-ray diffraction instrument with Cu K_α radiation (λ=1.5418 Å) (XRD, X'pert powder, Philips). Fourier transform infrared spectroscopy (FTIR) of the products was analyzed by a 170SX spectrometer in the range of 400-4000 cm^{-1}. Raman spectra were performed on an in Via Reinishaw confocal spectrometer with 633 nm laser. The surface composition and oxidation state of the products was obtained by the X-ray photoelectron spectroscopy (XPS, ESCALAB210). The magnetic properties of the products were studied by vibrating

Journal of Materials Chemistry C Accepted Manuscript

sample magnetometer (VSM, Lake Shore 7,304). Electron spin resonance (ESR) spectrum of the products was recorded at room temperature in X-band (8.984 GHz) by a JES-FA300 spectrometer (JEOL).

2.5 Electromagnetic measurements

The electromagnetic wave absorption properties of the bare Fe_3O_4 nanocrystals and Fe_3O_4/graphene hybrids were investigated by a network analyzer (Agilent Technologies E8363B) in the frequency range of 0.1-18 GHz by coaxial wire method. The composite samples for electromagnetic wave absorption measurement were fabricated by mixing paraffin with 50 wt% samples and pressed into toroidal shape (ψ_{out}: 7.00 mm, ψ_{in}: 3.04 mm). The complex permeability and permittivity were computed from the experimental scattering parameters through the standard Nicholson-Rossand Weir theoretical calculations.[54]

3. Results and discussion

Formation process of the hydrophobic Fe_3O_4/graphene hybrids

Taking advantage of the multifunctional (bridging, reducing and capping) features of oleylamine, we reported a simple in situ thermal decomposition approach for the synthesis of hydrophobic Fe_3O_4/graphene hybrids. The whole formation process is schematically illustrated in Fig. 1. Hydrophobic Fe_3O_4/graphene hybrids were fabricated by in situ thermal decomposition of organometallic compounds in the presence of oleylamine-modified GO in high-boiling organic solvent, in which oleylamine acts as a linker and surfactant. First, oleylamine was chemically bonded with the oxygen-containing functional groups on the surface of GO nanosheets by

Journal of Materials Chemistry C Accepted Manuscript

ultrasound approach, forming oleylamine-modified GO nanosheets. Owing to the strong covalent interactions between the oxygenic groups of GO and amine groups of oleylamine, the colloidal suspensions of oleylamine-modified GO nanosheets show high stability. Then, organometallic compounds were absorbed and coordinated onto the oleylamine-modified GO nanosheets, which is due to the absorption interactions between the hydrophobic groups of oleylamine-modified GO and organometallic compounds. Finally, monodisperse Fe_3O_4 nanocrystals were anchored on the surface of oleylamine-modified GO nanotheets through a robust in situ thermal decomposition strategy, in which the nucleation and growth were completely separated by adjusting the aging temperature. Oleylamine acts as both the alternative reducing agent and capping agent, leading to the formation of monodispersed Fe_3O_4 nanocrystals. Besides, the hydrophobic Fe_3O_4/graphene hybrids show high stability against ultrasound. Oleylamine is also used as bridging agent and provides interfacial interactions between the graphene nanosheets and Fe_3O_4 nanocrystals.

Characterization of the hydrophobic Fe_3O_4/graphene hybrids

The crystallographic structure of Fe_3O_4/graphene hybrids was characterized by XRD, as shown in Fig. 2. The positions and relative intensities of all the diffraction peaks can be well indexed to the *Fd3m* cubic spinel structure of Fe_3O_4 (JCPDS card NO.22-1086). No other impurity phases were detected. The obvious sharp peaks indicate that the samples are high crystalline. The broadening effect of the diffraction peaks is due to the small crystalline structure of Fe_3O_4 nanocrystals. Based on the Scherer's formula, the grain size of Fe_3O_4 nanocrystals in the Fe_3O_4/graphene hybrids

Journal of Materials Chemistry C Accepted Manuscript

is estimated to be about 8 nm. No characteristic peaks of graphene (broad stacking peak at about 26 °) were observed, suggesting that the attachment of Fe_3O_4 nanocrystals could prevent the restack of the graphene and the graphene nanosheets are disordered in the Fe_3O_4/graphene hybrids.[55]

The morphologies of GO and Fe_3O_4/graphene hybrids were examined by SEM and TEM. The typical SEM images of GO and Fe_3O_4/graphene hybrids are shown in Fig. 3. The exfoliated GO powder shows 2D layered structures with crumpled flaky wrinkles (Fig. 3 (a)). After in situ growth, it is clearly seen that tiny Fe_3O_4 nanocrystals were uniformly modified the surface of graphene nanosheets, forming sandwich-like structures (Fig. 3 (b)).

Fig. 4 shows the typical TEM images of GO and Fe_3O_4/graphene hybrids. After re-disperse into hexane, GO was transferred onto the holey carbon film on the copper grid for TEM measurement. As shown in Fig. 4 (a) and (b), the GO shows typical crumpled paper-like structures with many wrinkles on the surface and scrolling on the edge of the nanosheets. Besides, the GO nanosheets are almost transparent, indicating that it is very thin. The selected area electron diffraction (SAED) pattern of GO is shown in the inset of Fig. 4 (a). The bright diffraction spots with two sets of six fold patterns indicate that the GO has high crystalline nature with a hexagonal closed-packed (HCP) phase structure. Fig. 4 (c) and (d) present the TEM images of Fe_3O_4/graphene hybrids at different magnifications. The translucent graphene nanosheets are uniformly decorated by tiny Fe_3O_4 nanocrystals without aggregation and no large vacancy is observed on the surface of graphene nanosheets. No Fe_3O_4

Journal of Materials Chemistry C Accepted Manuscript

nanocrystals are found on the carbon film of copper grid without graphene. These results suggest a possible chemical bonding attraction between the graphene nanosheets and Fe_3O_4 nanocrystals. The histogram of size distribution of Fe_3O_4 nanocrystals is shown in Fig. S3. The average diameter of the Fe_3O_4 nanocrystals is approximately 8 nm, which matches well with the crystalline size estimated by XRD pattern. This result indicates that each individual particle is a single crystal.[56] The histogram can be fitted with a Gaussian distribution with a 7% standard deviation, suggesting that the Fe_3O_4 nanocrystals on the graphene nanosheets are monodispersed with a narrow size distribution. The inset of Fig. 4 (c) shows the SAED pattern of Fe_3O_4/graphene hybrids. The bright and distinguishable diffraction rings suggest the high crystalline feature of the samples. The diffraction rings can be indexed to be (311), (400), (422), (511) and (440) lattice planes, demonstrating the formation of face-centered cubic (fcc) structure of Fe_3O_4, which is accordant with the XRD result. The inset of Fig. 4 (d) reveals the HRTEM image of individual Fe_3O_4 nanocrystals. The interplanar spacing distance for the Fe_3O_4 nanocrystals is measured to be 0.258 nm, which corresponds to the (311) crystallographic plane of Fe_3O_4.

To further determine the position of Fe_3O_4 nanocrystals decorated on the graphene nanosheets, HAADF-STEM technique was used to investigate the morphology of Fe_3O_4/graphene hybrids. HAADF-STEM image, sometimes called Z-contrast image (Z, the atom number), has been proved to be an ideal tool for the characterization of heterogeneous hybrids.[28,57] The Z-contrast image could provide a better distinction between Fe_3O_4 (average $Z \approx 16$) and C ($Z = 6$). Fig. 4 (e) and (f) show the

Journal of Materials Chemistry C Accepted Manuscript

HAADF-STEM images of Fe_3O_4/graphene hybrids with different magnifications. The Fe_3O_4 nanocrystals with larger average atom number present bright dots like star and the graphene nanosheets with lower atom number show relative grey color like cloud. It is clearly seen that the Fe_3O_4 nanocrystals are uniformly decorated on the graphene nanosheets without aggregation, which is consistent with the above TEM results.

Raman and FTIR spectroscopy were employed to characterize the chemical bonding and surface functionalities of GO and Fe_3O_4/graphene hybrids. Fig. 5 (a) shows the Raman spectra of GO and Fe_3O_4/graphene hybrids. Two characteristic peaks are observed at ~ 1340 cm^{-1} and ~ 1590 cm^{-1}, which correspond to the D and G band, respectively. The G band is attributed to the first-order scattering of E_{2g}-vibration mode, which corresponds to the in-plane vibration of sp^2 carbon domains in the hexagonal lattice of graphene nanosheets. The D band is associated to the K-point phonons of A_{1g} mode, which is due to the vibration of sp^3 carbon domains in the plane terminations of disordered graphite.[28] The intensity ratio of D and G band (I_D/I_G) is relative with the disordered structure of carbon. Compared with GO, the Fe_3O_4/graphene hybrids reveal an obviously enhanced value of I_D/I_G, suggesting that the presence of more numerous but smaller sp^2 carbon domain resulted from the reduction process of GO during the formation of Fe_3O_4/graphene hybrids. These results are further demonstrated by FTIR and XPS technologies as bellow.

The FTIR spectrum of Fe_3O_4/graphene hybrids is shown in Fig. 5 (b). The broad band located at 3425 cm^{-1} is attributed to the combination of O-H deformation vibrations in graphene and N-H stretching vibrations in the carboxamide bond. The

Journal of Materials Chemistry C Accepted Manuscript

peak at 1545 cm^{-1} is assigned to the combination of N-H deformation vibrations and C-N stretching vibrations in the carboxamide bond. The peak at 1170 cm^{-1} is resulted from the mixed C-N stretching and N-H bending vibrations in the amido bond. The peaks at 2918 and 2946 cm^{-1} are due to the asymmetric and symmetric stretching vibrations of $-CH_2$ groups of the long CH_2 chains of oleylamine. The peak at 1462 cm^{-1} is owing to the deformation vibration of $-CH_3$ groups in the edges of oleylamine and graphene. The peak at 594 cm^{-1} is associated to the stretching vibrations of Fe-O bonds in Fe_3O_4. All the results suggest that Fe_3O_4 nanocrystals are chemically bonded on the surface of graphene nanosheets using oleylamine as the linker by the amidation reaction.[58] Therefore, the Fe_3O_4/graphene hybrids can be easily dispersed in the nonpolar solvents and possess hydrophobic characteristics as shown in Fig. 5 (c). Besides, the hydrophobic Fe_3O_4/graphene hybrids dispersed in nonpolar solvent can be separated from the solvent by using an applied magnet (Fig. 5 (c)).

The chemical composition of the samples was further examined by XPS spectra, as shown in Fig. 6. Fig. 6 (a) shows the full scan XPS spectra of GO and Fe_3O_4/graphene hybrids. Three sharp peaks with binding energy at 285, 530 and 711 eV are associated to C 1s, O 1s and Fe 2p, respectively, suggesting the presence of C, O and Fe elements in the Fe_3O_4/graphene hybrids. To further study the electronic states of the elements, high-resolution XPS spectra are characterized. The Fe 2p spectrum of Fe_3O_4/graphene hybrids (Fig. 6 (b)) shows only two characteristic peaks at 711.4 and 725.1 eV, which are originated from Fe $2p_{3/2}$ and Fe $2p_{1/2}$, respectively. These results demonstrate the formation of Fe_3O_4 nanocrystals in the hybrids. In the O

Journal of Materials Chemistry C Accepted Manuscript

1s spectrum (Fig. 6 (c)), the binding energy for the peak of O 1s shifted from 532.6 eV in GO to 530.4 eV in Fe_3O_4/graphene hybrids, which is due to the lattice oxygen in Fe_3O_4. Fig. 6 (d) and (e) reveal the C 1s spectra of GO and Fe_3O_4/graphene hybrids, respectively. The C 1s spectrum of GO (Fig. 6 (d)) show four deconvoluted peaks with binding energy of 285.0, 286.1, 287.1 and 288.9 eV, which are associated to the C-C/C=C in aromatic rings, C-OH, C-O-C and C=O groups, respectively. For the Fe_3O_4/graphene hybrids, the peaks of C 1s spectrum (Fig. 6 (e)) are mainly due to the non-oxygenated carbon groups (C-C/C=C) and the relative area ratios of oxygenated functional groups (C-O-C/C=O) are obviously decreased, which demonstrate that the oxygenated functional groups were partly removed. The XPS results indicate that GO was reduced during the reaction process. The existed residual defects and groups during the reduction of GO may provide defect polarization relaxation and groups' electronic dipole polarization relaxation, which may be favorable for electromagnetic wave absorption applications.[59]

Magnetic properties of the hydrophobic Fe_3O_4/graphene hybrids

Fig. 7 (a) shows the magnetic hysteresis loops of the bare Fe_3O_4 nanocrystals and Fe_3O_4/graphene hybrids measured at room temperature. The saturation magnetization (M_s) of the bare Fe_3O_4 nanocrystals and Fe_3O_4/graphene hybrids is 63 and 46 emu g^{-1}, respectively, which is smaller than that of the corresponding bulk Fe_3O_4 (92 emu g^{-1}). These smaller M_s values are mainly due to the surface spin canting and dead magnetic layer on the Fe_3O_4 nanocrystals. Besides, in comparison with the bare Fe_3O_4 nanocrystals, the smaller M_s value is owing to the weight-fraction of non-magnetic

Journal of Materials Chemistry C Accepted Manuscript

graphene nanosheets.[31] The magnetic hysteresis loops for both the samples show S-like shape with no coercivity and remanence, indicating the superparamagnetism nature, which is believed to be beneficial for high-performance electromagnetic wave absorption materials working at high frequency range.[31]

To further determine the microscopic magnetic information of the Fe_3O_4/graphene hybrids, ESR spectra of GO, bare Fe_3O_4 nanocrystals and Fe_3O_4/graphene hybrids were performed at room temperature, as shown in Fig. 7 (b). The principle of ESR technology depends on the transition between Zeeman components of the electronic levels, which can be used to investigate the interactions of magnetic moment with the neighboring and more distant local environment.[52] The ESR spectrum of GO shows no resonance band with low signal-to-noise ratio, indicating its non-magnetic characteristic, which is accordant with that of the MWCNT.[52] The ESR spectra for both the bare Fe_3O_4 nanocrystals and Fe_3O_4/graphene hybrids reveal a nearly symmetric signal with resonance band at 306 and 310 mT, respectively, indicating the superparamagnetic characteristic of Fe_3O_4 nanocrystals at room temperature. The shifts of resonance band originated from the local electronic environment of the unpaired electrons. When Fe_3O_4 nanocrystals are chemically bonded onto the graphene nanosheets, the line width is obviously enhanced from 41 mT of Fe_3O_4 nanocrystals to 55 mT of Fe_3O_4/graphene hybrids. The broaden effect of line width for the Fe_3O_4/graphene hybrids is possibly due to the spin disorder originated from the antiferromagentic interactions between the neighboring spins in Fe_3O_4 nanocrystals. These results suggest that the graphene nanosheets can reduce the dipolar interactions

Journal of Materials Chemistry C Accepted Manuscript

between the Fe_3O_4 nanocrystals and make them easily align with the external magnetic field.[60] The ESR results indicate that the chemically bonded graphene nanosheets increase the exchange interactions and reduce the dipolar interactions between the Fe_3O_4 nanocrystals, leading to the change of magnetic moment.

Electromagnetic wave absorption performance of the hydrophobic Fe_3O_4/graphene hybrids

When the electromagnetic wave is incident on the single-layer absorber backed by a metal plate, part of the incident electomagnetic wave is consumed by the absorber, part is reflected from the air-absorber interface (front interface), and part is reflected from the absorber-metal interface (back interface). The consumption of the incident electromagnetic wave convert into heat and spread to the environment. If the electromagnetic wave absorption characteritic is strong enough, the reflected electromagnetic wave is so weak that cannot be detected.

The electromagnetic wave absorption properties were investigated by mixing 50 wt% of the samples with paraffin. The reflection loss (RL) curves of a single layer absorber backed by a metal plate were obtained according to the transmit line theory, which is calculated using the relative complex permeability and permittivity at a given frequency and absorber thickness as expressed by the following equations:[31]

$$RL = 20\log\left|\frac{Z_{in} - Z_0}{Z_{in} + Z_0}\right| \quad (1)$$

$$Z_{in} = Z_0\left(\mu_r/\varepsilon_r\right)^{1/2}\tanh\left\{j\left(2\pi fd/c\right)\left(\mu_r\varepsilon_r\right)^{1/2}\right\} \quad (2)$$

where Z_{in} is the input impendence of absorber, Z_0 is the impedance of air, μ_r is the relative complex permeability, ε_r is the relative complex permittivity, f is the

Journal of Materials Chemistry C Accepted Manuscript

frequency of electromagnetic wave, *d* is the thickness of absorber, and c is the velocity of light in vacuum. A RL value of -10 dB is comparable to 90% of electromagnetic wave absorption, which is considered to evaluate the electromagnetic wave absorption efficiency of absorbers.

Fig. 8 shows the three-dimensional representations of variations of the RL values versus frequency at different thicknesses for the bare Fe_3O_4 nanocrystals and hydrophobic Fe_3O_4/graphene hybrids. The absorption peaks for both the composites shift to low frequency range as the thickness increases. The RL values for the bare Fe_3O_4 nanocrystals (Fig. 8 (a)) can hardly reach -10 dB with the thickness range of 1.0-5.0 mm in the whole frequency range and the maximum RL value is only -4.4 dB. The weak absorption ability suggests that the bare Fe_3O_4 nanocrystals cannot be used for the practical electromagnetic wave absorption applications. When the superparamagnetic Fe_3O_4 nanocrystals are covalently decorated on the surface graphene nanosheets, the absorption properties of hydrophobic Fe_3O_4/graphene hybrids (Fig. 8 (b)) are tremendously enhanced. The RL values exceeding -10 dB can be achieved in wide frequency range of 4.6-18 GHz with the absorber thickness of 2.0-5.0 mm. A maximum RL value of -40 dB is obtained at 6.8 GHz with a matching thickness of 4.5 mm. The hydrophobic Fe_3O_4/graphene hybrids possess remarkable enhanced absorption characteristic from C to K_u band (4-18 GHz), peculiarly covering the whole X-band (8-12 GHz) and K_u-band (12-18 GHz) which is of great significance for the military radar and direct broadcast satellite (DBS) owing to the high resolution imaging and precision target identification.[40] These results indicate

Journal of Materials Chemistry C Accepted Manuscript

that the addition of graphene nanosheets is significant for the enhancement of absorption properties of hydrophobic Fe_3O_4/graphene hybrids, which has been demonstrated before.[61] Compared with the bare graphene (a maximum RL value of -6.9 dB)[59] and Fe_3O_4 nanocrystals (Fig. 8 (a)), the enhanced absorption performance of hydrophobic Fe_3O_4/graphene hybrids is attributed to the synergistic effect between light-weight graphene and superparamagnetic Fe_3O_4 nanocrystals. Accompanying with the hydrophobic characteristic, the Fe_3O_4/graphene hybrids prepared in this work are promised to be good candidate for electromagnetic wave absorption materials in future practical applications in particular environmental conditions such as raining.

To investigate the possible mechanism for the enhancement of electromagnetic wave absorption properties, the frequency dependence of complex permeability ($\mu_r = \mu' - j\mu''$) and permittivity ($\varepsilon_r = \varepsilon' - j\varepsilon''$) for the Fe_3O_4 nanocrystals and hydrophobic Fe_3O_4/graphene hybrids are measured. The real part of complex permeability (μ') and complex permittivity (ε') represent the storage capability of magnetic and electric energy, respectively. The imaginary part of (μ'' and ε'') is related to the dissipation capability of magnetic and electric energy, respectively. Fig. 9 (a) shows the frequency dependence of complex permeability for the bare Fe_3O_4 nanocrystals and hydrophobic Fe_3O_4/graphene hybrids. The real part (μ') of complex permeability for the bare Fe_3O_4 nanocrystals slowly decreases from 2.4 to 1.5 by increasing the frequency from 0.1 to 3.5 GHz, and then maintains at 1.5 with a slightly fluctuation in 3.5-18 GHz. For the hydrophobic Fe_3O_4/graphene hybrids, the μ' value reduced from 2.2 to 1.4 with the increase of frequency from 0.1 to 5 GHz, and maintains at 1.4 in

Journal of Materials Chemistry C Accepted Manuscript

the range of 5-18 GHz. It is clear that the μ' value of Fe_3O_4 nanocrystals is slightly reduced when they were embedded by graphene. This can be relied to the reduction of M_s value after combination with nonmagnetic graphene. The variation between the bare Fe_3O_4 nanocrystals and Fe_3O_4/graphene hybrids can be negligible. This is possibly due to the low weighted-fraction of nonmagnetic graphene. The low relative complex permeability can be attributed to the small sized of magnetic Fe_3O_4 nanocrystals as well as the Snoek limit at high frequency range. The imaginary part (μ'') curves for both the samples show a broad at about 1 GHz. According to the ferromagnetic resonance theory,[62] the natural resonance frequency (f_r) can be expressed by the following equations:

$$f_r = \frac{\gamma}{2\pi} H_{eff} \quad (3)$$

$$H_{eff} = \frac{4|K_1|}{3\mu_0 M_s} \quad (4)$$

Where $\gamma/2\pi$ is the gyromagnetic ratio (28 GHz T^{-1}), H_{eff} is the effective magnetic field, K_1 is the magnetocrystalline anisotropic coefficient for the Fe_3O_4 (-11.8×10^3 J m^{-3}) and $\mu_0 M_s$ is the saturation magnetization (0.68 T). The calculated natural resonance frequency based on the above equations is 0.95 GHz, which is accordant with the experimental data (≈ 1 GHz). This result suggests that the resonance band for both the samples is ascribed to natural resonance of Fe_3O_4. The broad resonance band is believed to induce strong magnetic loss capabilities, which is promised to enhance the electromagnetic wave absorption. The magnetic loss for magnetic absorption materials mainly originates from the magnetic hysteresis, domain-wall displacement,

Journal of Materials Chemistry C Accepted Manuscript

natural resonance, exchange resonance and eddy current effect.[63] The magnetic hysteresis loss is caused by the irreversible magnetization, which can be neglected due to the superparamagnetic characteristic of the samples in this work. The domain wall resonance usually located at much lower frequency range (1-100 MHz) in the multi-domain materials, indicating that the domain-wall resonance loss can be excluded due to the single domain characteristic of the Fe_3O_4 nanocrystals and gigahertz frequency. The eddy current loss is related to the electric conductivity (σ) and thickness of the samples, which can be evaluated by the following equations:[38]

$$\mu_r^{''}(\mu_r^{'})^{-2} f^{-1} = 2\pi\mu_0\sigma d^2 \quad (5)$$

where μ_0 is the permeability of vacuum. If the magnetic loss is only related to the eddy-current loss, the values of $\mu_r''(\mu_r')^{-2}f^{-1}$ should be constant with the variation of frequency. Fig. S4 shows the frequency dependence of $\mu_r''(\mu_r')^{-2}f^{-1}$ for the bare Fe_3O_4 nanocrystals and hydrophobic Fe_3O_4/graphene hybrids. For the bare Fe_3O_4 nanocrystals, the values of $\mu_r''(\mu_r')^{-2}f^{-1}$ are almost constant in the high frequency range of 4.5-18 GHz. The values of $\mu_r''(\mu_r')^{-2}f^{-1}$ for the hydrophobic Fe_3O_4/graphene hybrids are constant in relative narrow frequency region of 7-18 GHz. It is clear that the bare Fe_3O_4 nanocrystals have obvious eddy current effect, and the high frequency range of the eddy current effect decreases by the introduction of graphene. These results suggest that the magnetic loss in the hydrophobic Fe_3O_4/graphene hybrids is mainly originated from natural resonance in 0.1-7 GHz and eddy current effect in 7-18 GHz.

Fig. 9 (b) shows the frequency dependence of complex permittivity for the Fe_3O_4

Journal of Materials Chemistry C Accepted Manuscript

nanocrystals and hydrophobic Fe_3O_4/graphene hybrids. The real part (ε') and imaginary part (ε'') of the bare Fe_3O_4 nanocrystals are nearly independent on frequency, which are almost constant with only an inconspicuous undulation ($\varepsilon' \approx 4$ and $\varepsilon'' \approx 0.07$). It is clear that the ε'' value is almost zero in the whole frequency range, which suggests that the bare Fe_3O_4 nanocrystals have negligible dielectric loss. For the hydrophobic Fe_3O_4/graphene hybrids, the complex permittivity is extremely enhanced in the whole frequency range. The ε' and ε'' values decline from 18.3 to 5.1 and 5.6 to 2.1, respectively, 4.5 and 80 times larger than that of the bare Fe_3O_4 nanocrystals at 0.1 GHz. The enhancement of complex permittivity is related to the increased electric polarization and electrical conductivity by the existence of graphene in the Fe_3O_4/graphene hybrids, which is favorable for enhanced complex permittivity according to the free electron theory,[63] $\varepsilon_r'' \approx 1/2\pi\varepsilon_0\rho f$. The complex permittivity of the hydrophobic Fe_3O_4/graphene hybrids displays a gradually decreased tendency with the increase of frequency. This frequency dispersion behavior is related to the increased lagging behind of dipole polarization response with respect to the electric field change.[64] Impedance matching characteristic ($Z_{in} = Z_0(\mu_r/\varepsilon_r)^{1/2}$) is an important parameter for electromagnetic wave absorption.[52,65,66] The impedance characteristic of the absorber should approach that of the free space, resulting in zero reflection at the front surface of the absorber. However, the modulus of the ratio between the complex permeability and permittivity $|\mu_r/\varepsilon_r|$ for the Fe_3O_4/graphene hybrids is far away from unity, suggesting that the electromagnetic wave absorption of the Fe_3O_4/graphene hybrids is quite different from the traditional impedance

Journal of Materials Chemistry C Accepted Manuscript

matching condition.

Magnetic loss and dielectric loss are another two possible factors for electromagnetic wave absorption.[66-68] In order to investigate the dominating mechanism for the enhanced absorption properties of Fe_3O_4/graphene hybrids, the frequency dependent magnetic loss tangent ($\tan\delta_\mu = \mu''/\mu'$) and dielectric loss tangent ($\tan\delta_\varepsilon = \varepsilon''/\varepsilon'$) of bare Fe_3O_4 nanocrystals and Fe_3O_4/graphene hybrids are calculated, as shown in Fig. 10. With the introduction of graphene, the Fe_3O_4/graphene hybrids show similar low $\tan\delta_\mu$ but improved $\tan\delta_\varepsilon$. These results suggest that the lightweight graphene plays a key role on the improvement of dielectric loss, which is of great significance for the electromagnetic wave absorption. Moreover, the reduction process of GO may generate many defects in the carbon 2D lattice, resulting in high ε'' and improved dielectric loss.[31] In the whole frequency range, the values of $\tan\delta_\varepsilon$ are obviously larger than that of the $\tan\delta_\mu$, which indicate that dielectric loss plays a key role in the enhanced absorption properties of Fe_3O_4/graphene hybrids. Furthermore, the dielectric loss may also caused by the dipole polarization and interfacial polarization at microwave frequencies.[1,65] The Fe_3O_4 nanocrystals have numerous surface atoms with local breaking of symmetry due to the surface effect, causing increased diploes and dipole polarization. Besides, the well dispersed Fe_3O_4 nanocrystals anchored uniformly on the surface of graphene nanosheets may introduce more extra interfaces, leading to interfacial polarization and stronger associated relaxation occurred at the nanocrystals/graphene interfaces.[69] These polarization effects may also contribute an increase of dielectric loss.

Journal of Materials Chemistry C Accepted Manuscript

In addition, electromagnetic wave attenuation in the interior of absorber is an important key factor for a remarkable absorption material. The attenuation constant (α) determines the attenuation performance of materials, which can be denoted by the following formula:[65]

$$\alpha = \frac{\sqrt{2}\pi f}{c} \times \sqrt{\left(\mu''\varepsilon'' - \mu'\varepsilon'\right) + \sqrt{\left(\mu''\varepsilon'' - \mu'\varepsilon'\right)^2 + \left(\varepsilon'\mu'' + \varepsilon''\mu'\right)^2}} \quad (6)$$

where f is the frequency of the electromagnetic wave and c is the velocity of light. The frequency dependence of α for the bare Fe_3O_4 nanocrystals and Fe_3O_4/graphene hybrids is displayed in Fig. 11. In is clearly seen that the Fe_3O_4/graphene hybrids have larger α in the entire frequency range, suggesting that the better attenuation performance of materials.

The absorber thickness is one of the critical parameters, which determines the intensity and position of the maximum RL value. To investigate the physical phenomenon, the quarter-wavelength matching model ($\lambda/4$) was adopted, in which the maximum RL can be achieved at a certain frequency if the absorber thickness satisfies by the following equation:[21,31]

$$t_m = \frac{n\lambda}{4} = \frac{nc}{4 f_m \sqrt{|\mu_r||\varepsilon_r|}} \quad (n=1, 3, 5,\ldots) \quad (7)$$

where t_m is the thickness of absorber, λ is the wavelength of the electromagnetic wave, f_m is the peak frequency of the maximum RL, $|\mu_r|$ and $|\varepsilon_r|$ are respectively the modulus of the measured μ_r and ε_r at f_m, and c is the velocity of light in a vacuum. According to the quarter-wavelength matching condition, when the absorber thickness satisfies the formula (7), the two energing reflected electromagnetic wave from the air-absorber

Journal of Materials Chemistry C Accepted Manuscript

interface and absorber-metal interface are out of phase by 180 º, leading to an extinction of them on the air-absorber interface. Fig. 12 (a) reveals the variations of RL curves versus frequency of the Fe_3O_4/graphene hybrids at ten thicknesses. Based on the quarter wavelength model, a simulation of the thickness (t_m) versus peak frequency (f_m) for the Fe_3O_4/graphene hybrids is displayed in Fig. 12 (b). The red stars are the matching thicknesses (denoted as t_m^{exp}) versus the peak frequency (f_m), which were directly achieved from the RL curves in Fig. 12 (a). Obviously, the red stars are exactly located around the $\lambda/4$ curve, which suggests that the relationship between matching thickness and peak frequency for the electromagnetic wave absorption of Fe_3O_4/graphene hybrids obeys the quarter-wavelength matching condition. Furthermore, the quarter-wavelength matching theory is believed to be of great significance to guide the design of absorber thickness for electromagnetic wave absorption, once the corresponding complex permeability and permittivity are obtained.

Conclusions

In summary, a facile in situ thermal decomposition route is developed to fabricate hydrophobic Fe_3O_4/graphene hybrids, in which monodispersed superparamagnetic Fe_3O_4 nanocrystals are uniformly decorated and chemically bonded on the graphene nanosheets without aggregation or large vacancies. In comparison with the bare Fe_3O_4 nanocrystals and graphene, the hydrophobic Fe_3O_4/graphene hybrids show enhanced electromagnetic wave absorption characteristic. The hydrophobic Fe_3O_4/graphene hybrids show a maximum RL value of -40 dB at 6.8 GHz with a matching thickness

Journal of Materials Chemistry C Accepted Manuscript

of 4.5 mm and a broad bandwidth (RL ≤ -10 dB) in 4.6-18 GHz range for the thicknesses of 2.0-5.0 mm. Such enhanced absorption properties of the Fe_3O_4/graphene hybrids is ascribed to the synergistic effect of superparamagnetic Fe_3O_4 nanocrystals and light-weight graphene, including magnetic loss from superparamangetic Fe_3O_4 nanocrystals, dielectric loss from the light weight graphene, interfacial polarization between the Fe_3O_4 nanocrystals and graphene, and high attenuation efficiency. The relationship between absorber thickness and frequency of the absorption peak for the Fe_3O_4/graphene hybrids obeys the quarter-wavelength matching theory, facilitating the design of absorber thickness for electromagnetic wave absorption. Moreover, the hydrophobic characteristic is believed to be more stable and suitable to be applied in some particular environmental conditions. These results suggest that the hydrophobic Fe_3O_4/graphene hybrids have great potential for the manufacture of electromagnetic wave-absorbing devices with light weight, high efficiency and adaptability to environment. In addition, the facile synthesis of hydrophobic Fe_3O_4/graphene hybrids presented in this work also opens the opportunities to prepare other functional nanoparticle/graphene hybrid systems with hydrophobic characteristic for future industrial applications.

Acknowledgements

This work was supported by the grants from the Natural Science Foundation of Shannxi Province, China (2014JQ1040), Foundation of Educational department of Shaanxi Province, China (14JK1727) and the Science Foundation of Northwest University (13NW13).

Journal of Materials Chemistry C Accepted Manuscript

References

1 B. Wen, M. S. Cao, M. M. Lu, W. Q. Cao, H. L. Shi, J. Liu, X. X. Wang, H. B. Jin, X. Y. Fang, W. Z. Wang, J. Yuan, *Adv. Mater.*, 2014, **26**, 3484.

2 J. W. Liu, R. C. Che, H. J. Chen, F. Zhang, F. Xia, Q. S. Wu, M. Wang, *Small*, 2012, **8**, 1214.

3 G. Z. Wang, Z. Gao, S. W. Tang, C. Q. Chen, F. F. Duan, S. C. Zhao, S. W. Lin, Y. H. Feng, L. Zhou, Y. Qin, *ACS Nano*, 2012, **6**, 11009.

4 W. L. Song, J. Wang, L. Z. Fan, Y. Li, C. Y. Wang, M. S. Cao, *ACS Appl. Mater. Interfaces*, 2014, **6**, 10516.

5 X. A. Fan, J. G. Guan, Z. Z. Li, F. Z. Mou, G. X. Tong, W. Wang, *J. Mater. Chem.*, 2010, **20**, 1676.

6 C. Wang, X. J. Han, X. L. Zhang, S. R. Hu, T. Zhang, J. Y. Wang, Y. C. Du, X. H. Wang, P. Xu, *J. Phys. Chem. C*, 2010, **114**, 14826.

7 G. X. Tong, Q. Hu, W. H. Wu, W. Li, H. S. Qian, Y. Liang, *J. Mater. Chem.*, 2012, ***22***, 17494.

8 R. L. Ji, C. B. Cao, Z. Chen, H. Z. Zhai, J. Bai, *J. Mater. Chem. C*, 2014, **2**, 5944.

9 G. S. Wang, Y. Y. Wu, X. J. Zhang, Y. Li, L. Guo, M. S. Cao, *J. Mater. Chem. A*, 2014, **2**, 8644.

10 S. W. Phang, M. Tadokoro, J. Watanabe, N. Kuramoto, *Curr. Appl. Phys.*, 2008, **8**, 391.

11 G. S. Wang, S. He, X. Luo, B. Wen, M. M. Lu, L. Guo, M. S. Cao, *RSC Adv.*, 2013, **3**, 18009.

Journal of Materials Chemistry C Accepted Manuscript

12 S. He, G. S. Wang, C. Lu, J. Liu, B. Wen, H. Liu, L. Guo, M. S. Cao, *J. Mater. Chem. A*, 2013, **1**, 4685.

13 Y. F. Zhu, L. Zhang, T. Natsuki, Y. Q. Fu, Q. Q. Ni, *ACS Appl. Mater. Interfaces*, 2012, **4**, 2101.

14 H. L. Yu, T. S. Wang, B. Wen, M. M. Lu, Z. Xu, C. L. Zhu, Y. J. Chen, X. Y. Xue, C. W. Sun, M. S. Cao, *J. Mater. Chem.*, 2012, **22**, 21679.

15 H. J. Yang, M. S. Cao, Y. Li, H. L. Shi, Z. L. Hou, X. Y. Fang, H. B. Jin, W. Z. Wang, J. Yuan, *Adv. Optical Mater.*, 2014, **2**, 214.

16 B. Wen, M. S. Cao, Z. L. Hou, W. L. Song, L. Zhang, M. M. Lu, H. B. Jin, X. Y. Fang, W. Z. Wang, J. Yuan, *Carbon*, 2013, **65**, 124.

17 Z. J. Wang, L. N. Wu, J. G. Zhou, B. Z. Shen, Z. H. Jiang, *RSC Adv.*, 2013, **3**, 3309.

18 N, K. Sun, B. S. Du, F. Liu, P. Z. Si, M. X. Zhao, X. Y. Zhang, G. M. Shi, *J. Alloys Compd.*, 2013, **577**, 533.

19 G. Q. Wang, L. X. Ma, Y. F. Chang, C. Liu, *Appl. Sur. Sci.*, 2012, **258**, 3962.

20 J. Zheng, Z. X. Yu, G. B. Ji, X. H. Lin, H. L. Lv, Y. W. Du, *J. Alloys Compd.*, 2014, **602**, 8.

21 F. S. Wen, F. Zhang, Z. Y. Liu, *J. Phys. Chem. C*, 2011, **115**, 14025.

22 R. C. Che, L.M. Peng, X. F. Duan, Q. Chen, X. L. Liang, *Adv. Mater.*, 2004, **16**, 401.

23 X. G. Liu, S. W. Or, S. L. Ho, C. C. Cheung, C. M. Leung, Z. Han, D. Y. Geng, Z. D. Zhang, *J. Alloys Compd.*, 2011, **509**, 9071.

Journal of Materials Chemistry C Accepted Manuscript

24 X. S. Qi, Y. Yang, W. Zhong, C. Qin, Y. Deng, C. Au, Y. W. Du, *Carbon*, 2010, **48**, 3512.

25 V. K. Singh, A. Shukla, M. K. Patra, L. Saini, R. K. Jani, S. R. Vadera, N. Kumar, *Carbon*, 2012, **50**, 2202.

26 X. Huang, Z. Y. Yin, S. X. Wu, X. Y. Qi, Q. Y. He, Q. C. Zhang, Q. Y. Yan, F. Boey, H. Zhang, *Small*, 2011, **7**, 1876.

27 Y. Huang, J. J. Liang, Y. S. Chen, *Small*, **8**, 1805.

28 X. H. Li, H. Zhu, J. Feng, J. W. Zhang, X. Deng, B. F. Zhou, H. L. Zhang, D. S. Xue, F. S. Li, N. J. Mellors, Y. F. Li, Y. Peng, *Carbon*, 2013, **60**, 488.

29 S. Bai, X. P. Shen, *RSC Adv.*, 2012, **2**, 64.

30 X. J. Zhang, G. S. Wang, W. Q. Cao, Y. Z. Wei, J. F. Liang, L. Guo, M. S. Cao, *ACS Appl. Mater. Interfaces*, 2014, **6**, 7471.

31 X. H. Li, J. Feng, H. Zhu, C. H. Qu, J. T. Bai, X. L. Zheng, *RSC Adv.*, 2014, **4**, 33619.

32 P. B. Liu, Y. Huang, X. Sun, *ACS Appl. Mater. Interfaces*, 2013, **5**, 12355.

33 X. Sun, J. P. He, G. X. Li, J. Tang, T. Wang, Y. X. Guo, H. R. Xue, *J. Mater. Chem. C*, 2013, **1**, 765.

34 D. Z. Chen, G. S. Wang, S. He, J. Liu, L. Guo, M. S. Cao, *J. Mater. Chem. A*, 2013, **1**, 5996.

35 Y. J. Chen, Z. Y. Lei, H. Y. Wu, C. L. Zhu, P. Gao, Q. Y. Ouyang, L. H. Qi, W. Qin, *Mater. Res. Bull.*, 2013, **48**, 3362.

36 X. H. Li, J. Feng, Y. P. Du, J. T. Bai, H. M. Fan, H. L. Zhang, Y. Peng, F. S. Li, *J.*

Journal of Materials Chemistry C Accepted Manuscript

Mater. Chem. A, 2015, **3**, DOI: 10.1039/C4TA05718J

37 H. T. Zhao, Z. G. Li, N. Zhang, Y. C. Du, S. W. Li, L. Shao, D. Y. Gao, X. J. Han, P. Xu, *RSC Adv.*, 2014, **4**, 30467.

38 G. Z. Wang, Z. Gao, G. P. Wan, S. W. Lin, P. Yang, Y. Qin, *Nano Res.*, 2014, **7**, 704.

39 C. G. Hu, Z. Y. Mou, G. W. Lu, N. Chen, Z. L. Dong, M. J. Hu and L. T. Qu, *Phys. Chem. Chem. Phys.*, 2013, **15**, 13038.

40 X. H. Li, H. B. Yi, J. W. Zhang, J. Feng, F. S. Li, D. S. Xue, H. L. Zhang, Y. Peng and N. J. Mellors, *J. Nanopart. Res.*, 2013, **15**, 1472.

41 C. G. Hu, Z. Y. Mou, G. W. Lu, N. Chen, Z. L. Dong, M. J. Hu, L. T. Qu, *Phys. Chem. Chem. Phys.*, 2013, **15**, 13038.

42 H. L. Xu, H. Bi, R. B. Yang, *J. Appl. Phys.*, 2012, **111**, 07A522.

43 M. Zong, Y. Huang, Y. Zhao, L. Wang, P. B. Liu, Y. Wang, Q. F. Wang, *Mater. Lett.*, 2013, **106**, 22.

44 J. Zheng, H. L. Lv, X. H. Lin, G. B. Ji, X. G. Li, Y. W. Du, *J. Alloy. Compd.*, 2014, **589**, 174.

45 T. S. Wang, Z. H. Liu, M. M. Lu, B. Wen, Q. Y. Ouyang, Y. J. Chen, C. L. Zhu, P. Gao, C. Y. Li, M. S. Cao, L. H. Qi, *J. Appl. Phys.*, 2013, **113**, 024314.

46 E. L. Ma, J. J. Li, N. Q. Zhao, E. Z. Liu, C. N. He, C. S. Shi, *Mater. Lett.*, 2013, **91**, 209.

47 Y. L. Ren, C. L. Zhu, S. Zhang, C. Y. Li, Y. J. Chen, P. Gao, P. P. Yang, Q. Y. Ouyang, *Nanoscale*, 2013, **5**, 12296.

Journal of Materials Chemistry C Accepted Manuscript

48 Y. L. Ren, H. Y. Wu, M. M. Lu, Y. J. Chen, C. L. Zhu, P. Gao, M. S. Cao, C. Y. Li, Q. Y. Ouyang, *ACS Appl. Mater. Interfaces*, 2012, **4**, 6436.

49 Y. L. Ren, C. L. Zhu, L. H. Qi, H. Gao, Y. J. Chen, *RSC Adv.*, 2014, **4**, 21510.

50 H. M. Zhang, C. L. Zhu, Y. J. Chen, H. Gao, *ChemPhysChem*, 2014, **15**, 2261.

51 C. Y. Liang, C. Y. Liu, H. Wang, L. N. Wu, Z. H. Jiang, Y. J. Xu, B. Z. Shen, Z. J. Wang, *J. Mater. Chem. A*, 2014, **2**, 16397.

52 Z. J. Wang, L. N. Wu, J. G. Zhou, W. Cai, B. Z. Shen, Z. H. Jiang, *J. Phys. Chem. C*, 2013, **117**, 5446.

53 W. S. Hummers, R. E. Offeman, *J. Am. Chem. Soc.*, 1958, **80**, 1339.

54 A. M. Nicolson, G. F. Ross, *IEEE Trans. Instrum. Meas.*, 1970, **19**, 377.

55 C. Xu, X. Wang, J. W. Zhu, *J. Phys. Chem. C*, 2008, **112**, 19841.

56 X. H. Li, G. G. Tan, W. Chen, B. F. Zhou, D. S. Xue, Y. Peng, F. S. Li, N. J. Mellors, *J. Nanopart. Res.*, 2012, **14**, 751.

57 J. C. González, J. C. Hernández, M. López-Haro, E. del Río, J. J. Delgado, A. B. Hungría, S. Trasobares, S. Bernal, P. A. Midgley and J. J. Calvino, *Angew. Chem. Int. Ed.*, 2009, **48**, 5313.

58 F. He, J. T. Fan, D. Ma, L. M. Zhang, C. Leung, H. L. Chan, *Carbon*, 2010, **48**, 3139.

59 C. Wang, X. J. Han, P. Xu, X. L. Zhang, Y. C. Du, S. R. Hu, J. Y. Wang, X. H. Wang, *Appl. Phys. Lett.*, 2011, **98**, 072906.

60 K. M. Kant, K. Sethupathi, M. S. R. Rao, *J. Appl. Phys.*, 2008, **103**, 07D501.

61 B. Wen, X. X. Wang, W. Q. Cao, H. L. Shi, M. M. Lu, G. Wang, H. B. Jin, W. Z.

Journal of Materials Chemistry C Accepted Manuscript

Wang, J. Yuan, M. S. Cao, *Nanoscale*, 2014, **6**, 5754.

62 C. Kittel, *Phys. Rev.*, 1948, **73**, 155.

63 Y. C. Du, W. W. Liu, R. Qiang, Y. Wang, X. J. Han, J. Ma, P. Xu, *ACS Appl. Mater. Interfaces*, 2014, **6**, 12997.

64 H. Wang, Y. Y. Dai, W. J. Gong, D. Y. Geng, S. Ma, D. Li, W. Liu, *Appl. Phys. Lett.*, 2013, **102**, 223113.

65 J. Xiang, J. L. Li, X. H. Zhang, Q. Ye, J. H. Xu, X. Q. Shen, *J. Mater. Chem. A*, 2014, **2**, 16905.

66 M. S. Cao, R. R. Qin, C. J. Qiu, J. Zhu, *Mater. Des.*, 2003, **24**, 391.

67 M. S. Cao, J. Yang, W. L. Song, D. Q. Zhang, B. Wen, H. B. Jin, Z. L. Hou, J. Yuan, *ACS Appl. Mater. Interfaces*, 2012, **4**, 6949.

68 M. M. Lu, W. Q. Cao, H. L. Shi, X. Y. Fang, J. Yang, Z. L. Hou, H. B. Jin, W. Z. Wang, J. Yuan, M. S. Cao, *J. Mater. Chem. A*, 2014, **2**, 10540.

69 Y. J. Chen, G. Xiao, T. S. Wang, Q. Y. Ouyang, L. H. Qi, Y. Ma, P. Gao, C. L. Zhu, M. S. Cao, H. B. Jin, *J. Phys. Chem. C*, 2011, **115**, 13603.

Journal of Materials Chemistry C Accepted Manuscript

Figure captions

Fig. 1 Schematic illustration for the formation of the hydrophobic Fe_3O_4/graphene hybrids and their application for electromagnetic wave absorption.

Fig. 2 XRD patterns of the Fe_3O_4/graphene hybrids.

Fig. 3 SEM images of (a) GO and (b) Fe_3O_4/graphene hybrids.

Fig. 4 TEM images of (a, b) GO and (c, d) Fe_3O_4/graphene hybrids. Insets of Fig. 3 (a), (c) and (d) show the SAED pattern of GO, SAED pattern of Fe_3O_4/graphene hybrids and HRTEM image a single Fe_3O_4 nanocrystal in the Fe_3O_4/graphene hybrids, respectively; (e, f) HAADF-STEM images of Fe_3O_4/graphene hybrids.

Fig. 5 (a) Raman spectra of GO and Fe_3O_4/graphene hybrids; (b) FTIR spectra of Fe_3O_4/graphene hybrids; (c) schematic of the hydrophobic characteristic and magnetic separation of Fe_3O_4/graphene hybrids.

Fig. 6 XPS spectra: (a) wide scan of GO and Fe_3O_4/graphene, (b) Fe2p spectra of Fe_3O_4/graphene, (c) C1s spectra of GO, (d) C1s spectra of Fe_3O_4/graphene, and (e) O1s spectra of GO and Fe_3O_4/graphene

Fig. 7 (a) Magnetic hysteresis loops of the bare Fe_3O_4 nanocrystals and Fe_3O_4/graphene hybrids; (b) ESR spectra of GO, bare Fe_3O_4 nanocrystals and Fe_3O_4/graphene hybrids.

Fig. 8 Three-dimensional representation of RL values for the paraffin-based composites (50 wt%): (a) pure Fe_3O_4 nanocrystals and (b) Fe_3O_4/GO hybrids.

Fig. 9 The frequency dependence of (a) complex permeability and (b) complex permittivity for the bare Fe_3O_4 nanocrystals and hydrophobic Fe_3O_4/graphene hybrids

Journal of Materials Chemistry C Accepted Manuscript

Fig. 10 Frequency dependence of (a) magnetic loss tangent and (b) dielectric loss tangent for bare Fe_3O_4 nanocrystals and Fe_3O_4/graphene hybrids.

Fig. 11 Frequency dependence of attenuation constant for bare Fe_3O_4 nanocrystals and Fe_3O_4/graphene hybrids.

Fig. 12 (a) Frequency dependence of RL curves for the Fe_3O_4/graphene hybrids (50 wt%) with ten thicknesses; (b) simulations of the absorber thickness (t_m) versus peak frequency (f_m) for the Fe_3O_4/graphene hybrids (50 wt%) under λ/4 model.

Journal of Materials Chemistry C Accepted Manuscript

Fig. 1

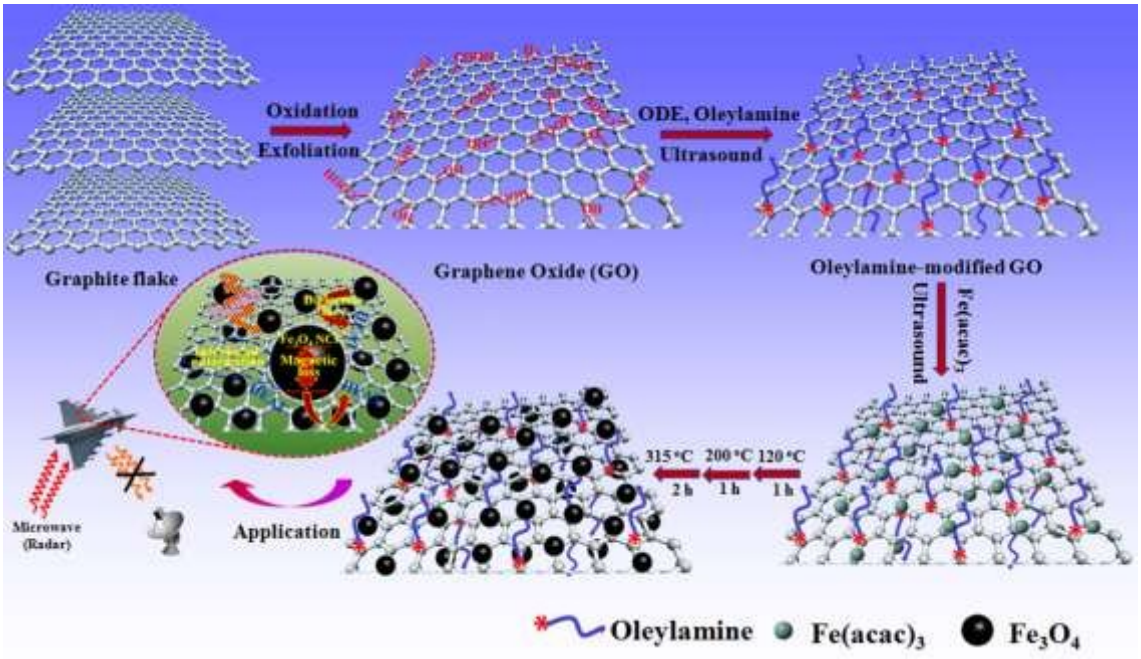

Journal of Materials Chemistry C Accepted Manuscript

Fig. 2

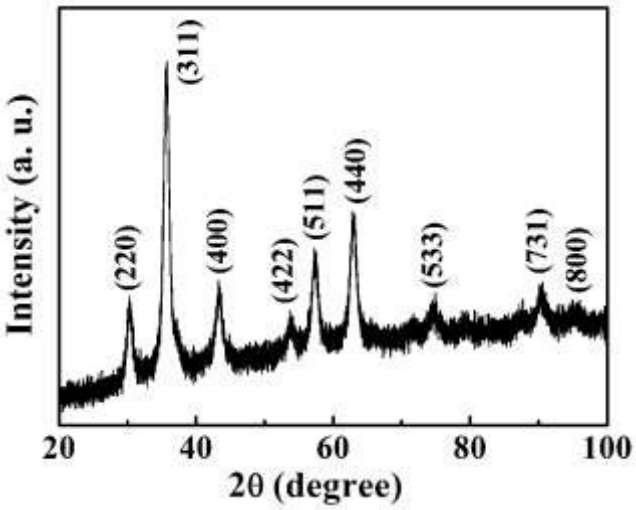

Journal of Materials Chemistry C Accepted Manuscript

Fig. 3

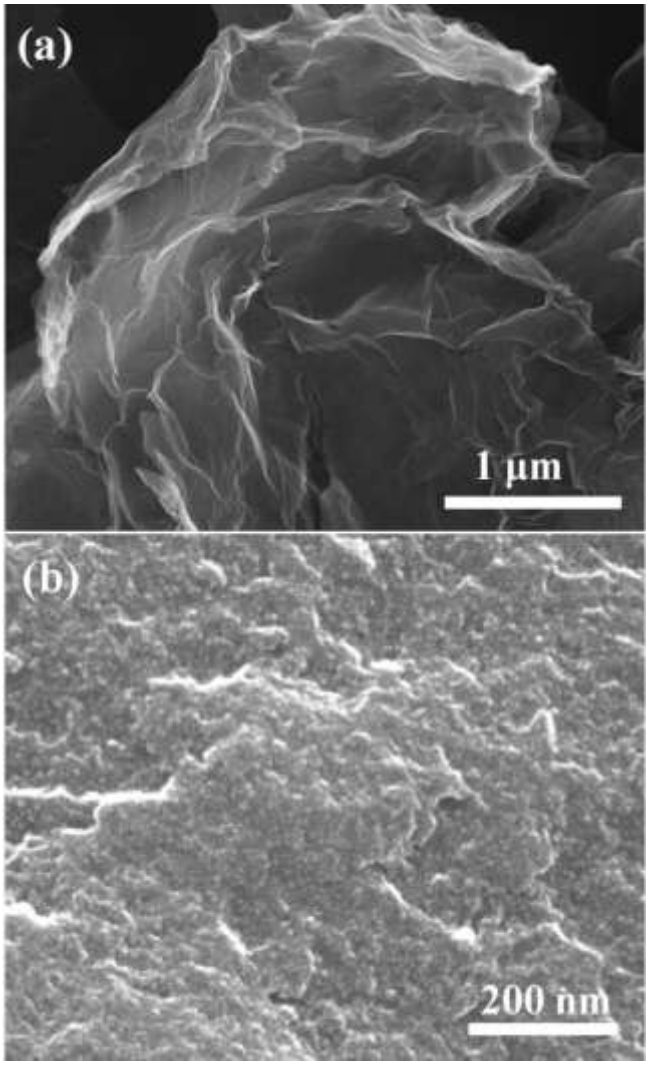

Journal of Materials Chemistry C Accepted Manuscript

Fig. 4

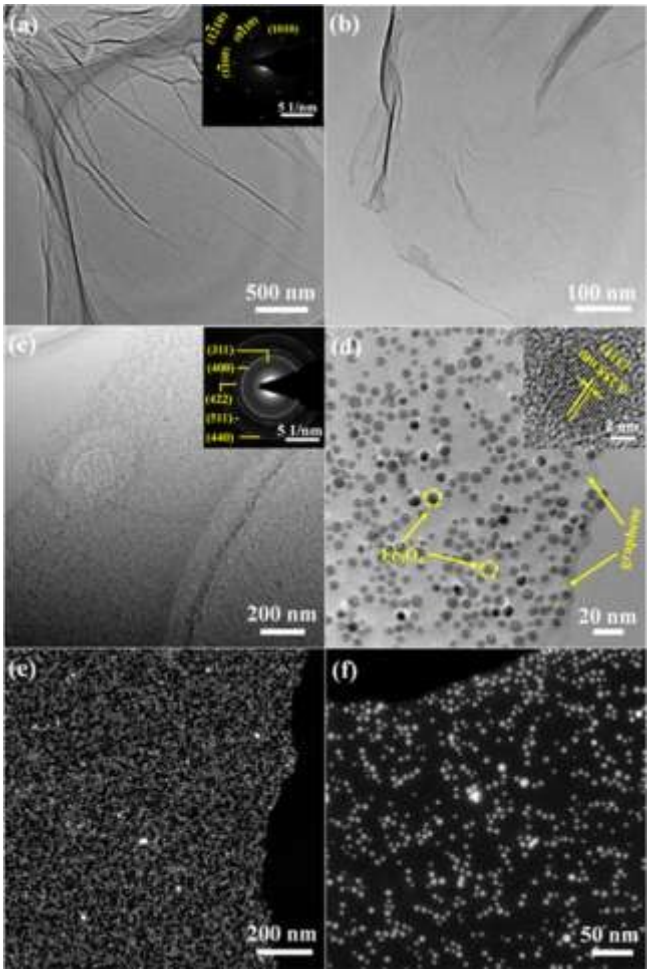

Journal of Materials Chemistry C Accepted Manuscript

Fig. 5

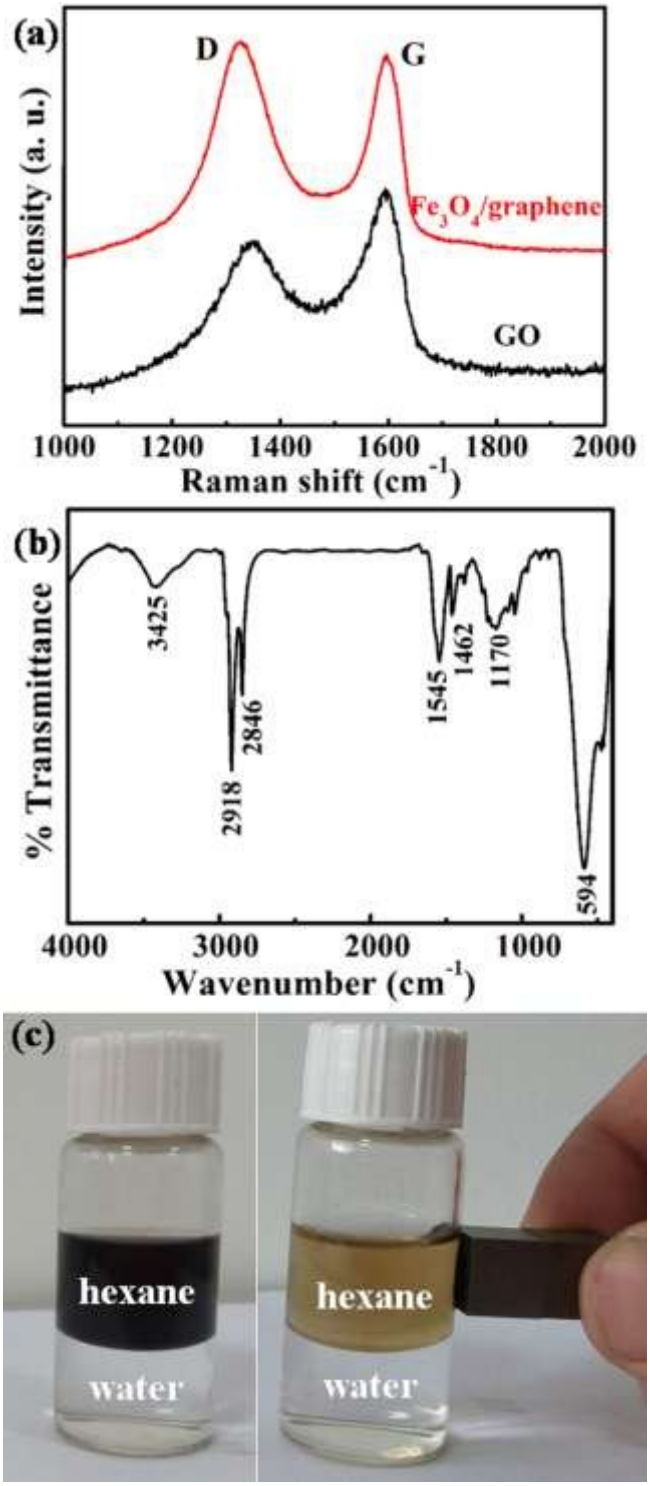

Journal of Materials Chemistry C Accepted Manuscript

Fig. 6

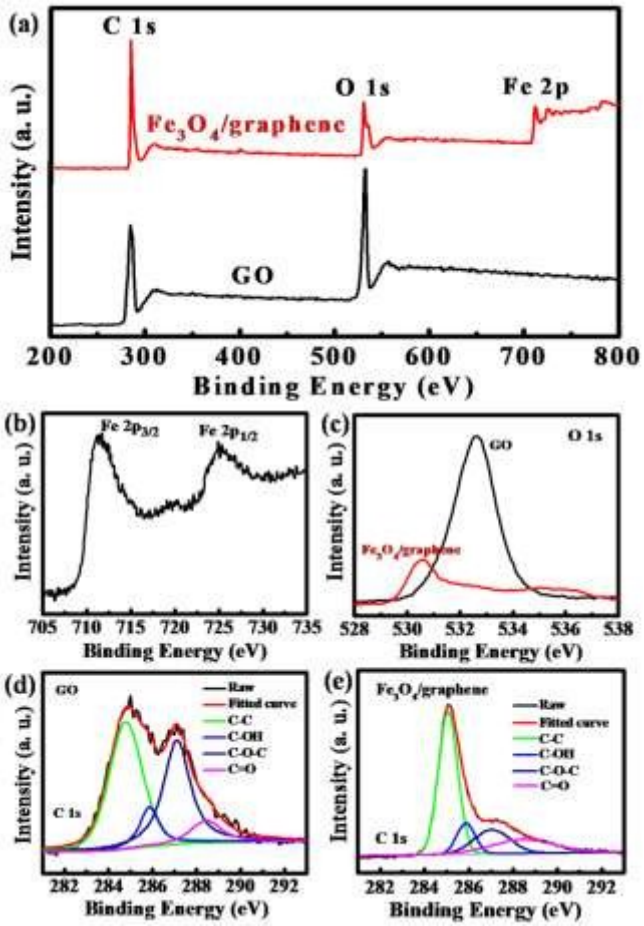

Journal of Materials Chemistry C Accepted Manuscript

Fig. 7

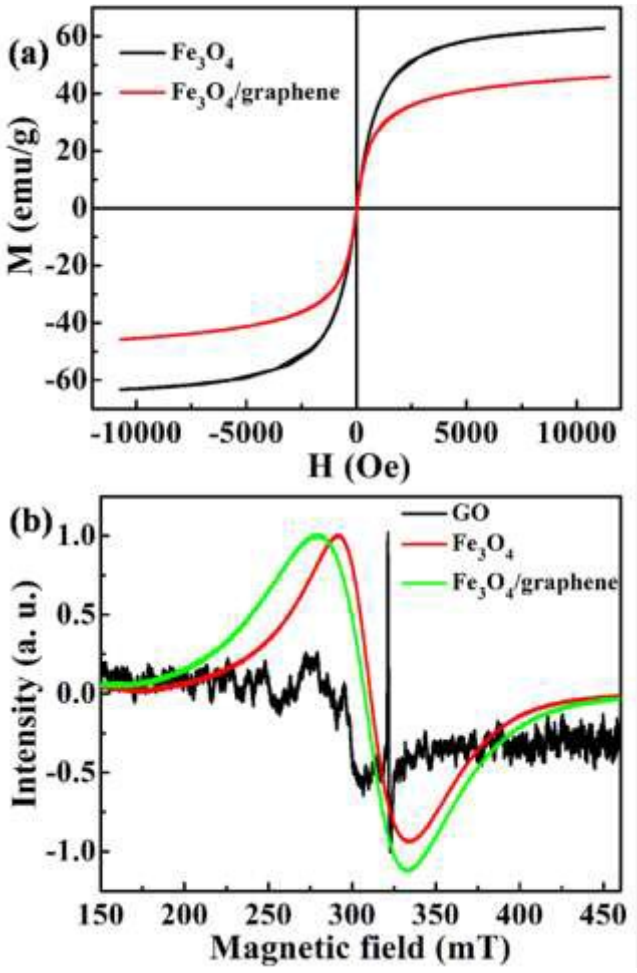

Journal of Materials Chemistry C Accepted Manuscript

Fig. 8

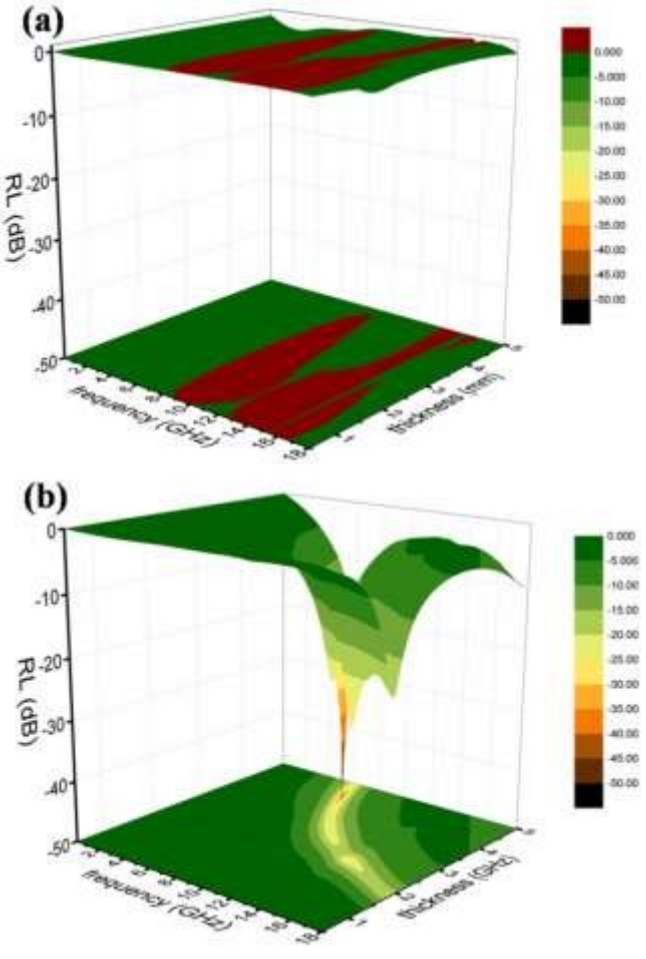

Journal of Materials Chemistry C Accepted Manuscript

Fig. 9

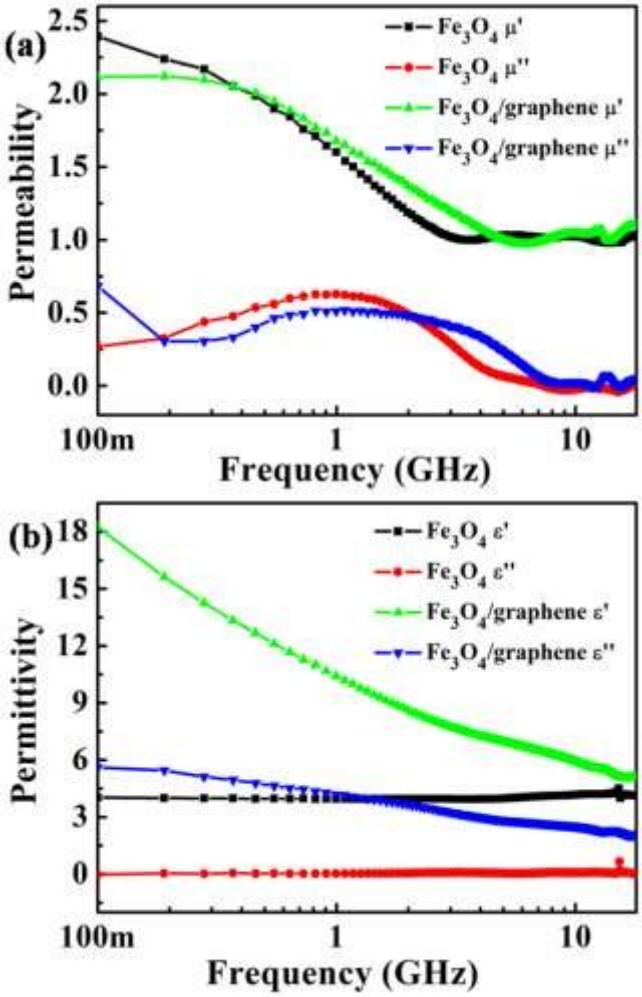

Journal of Materials Chemistry C Accepted Manuscript

Fig. 10

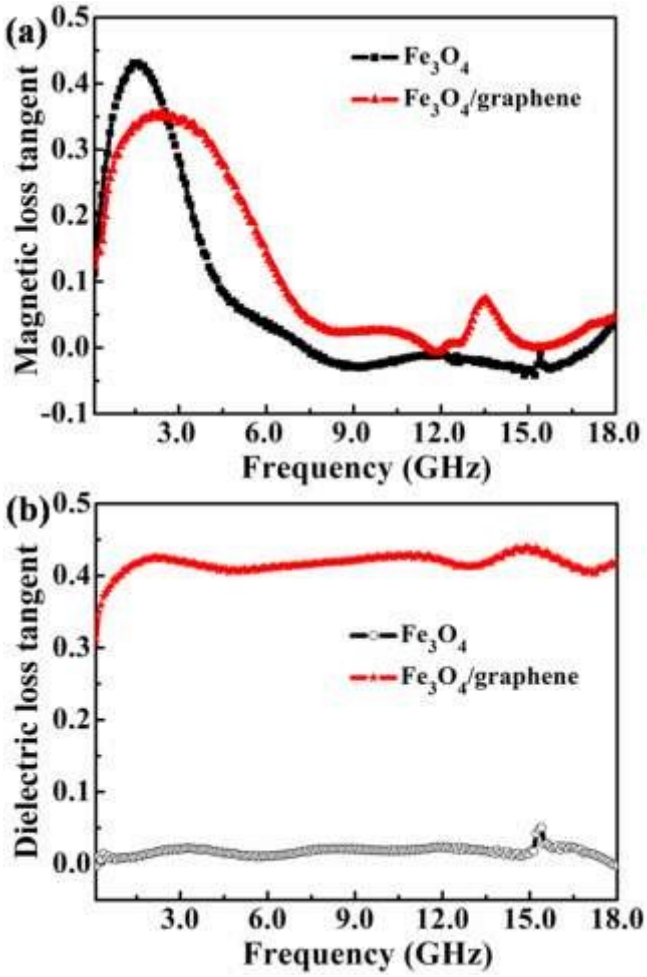

Journal of Materials Chemistry C Accepted Manuscript

Fig. 11

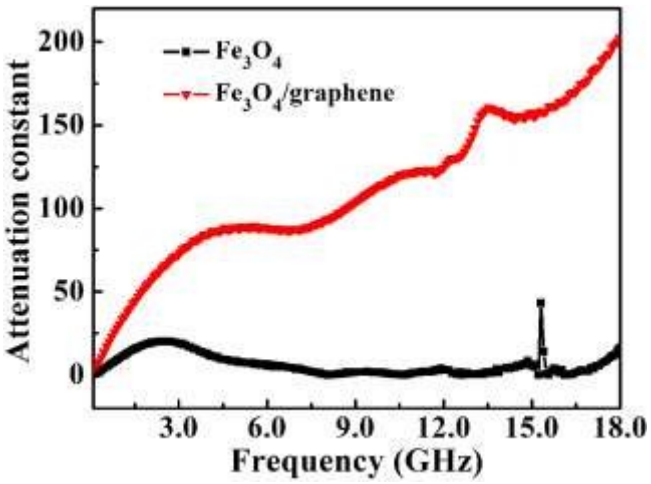

Journal of Materials Chemistry C Accepted Manuscript

Fig. 12

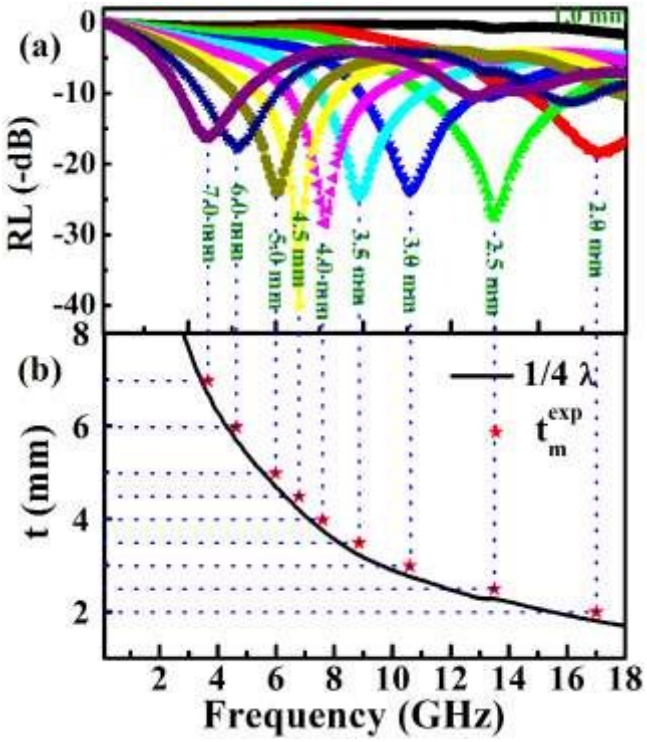

Journal of Materials Chemistry C Accepted Manuscript

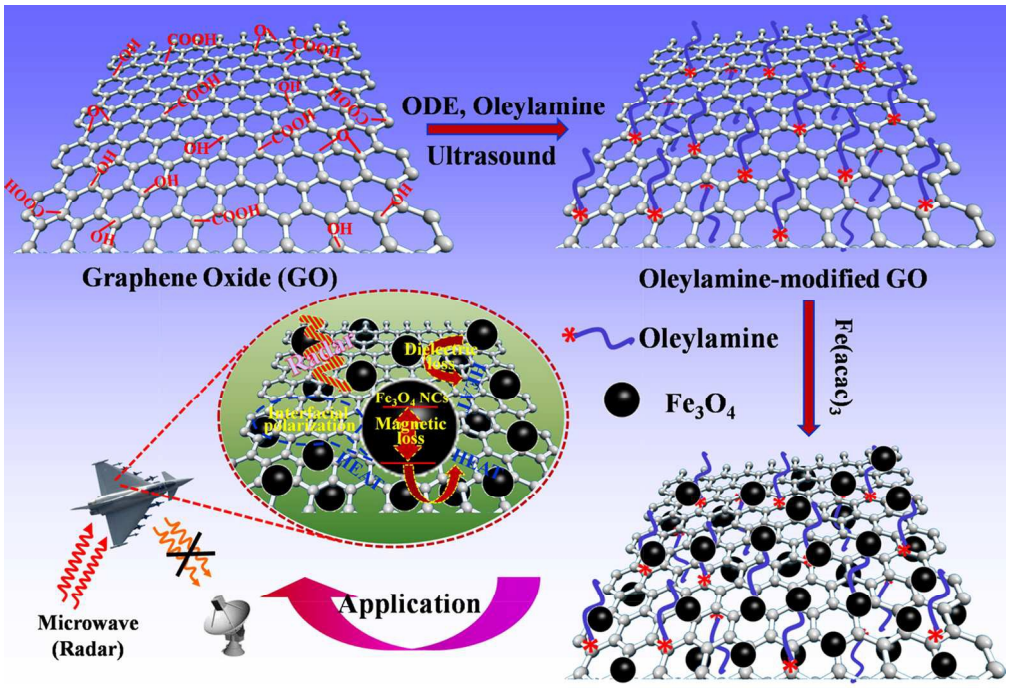

119x82mm (300 x 300 DPI)

Journal of Materials Chemistry C Accepted Manuscript